Environ. Sci. Technol. **2008,** *42,* 896–900

Two Dimensional Transport Characteristics of Surface Stabilized Zero-valent Iron Nanoparticles in Porous Media

S. R. KANEL, R. R. GOSWAMI, T. P. CLEMENT,* M. O. BARNETT, AND D. ZHAO

Department of Civil Engineering, Auburn University, Auburn, Alabama 36849

Received July 18, 2007. Revised manuscript received November 13, 2007. Accepted November 15, 2007.

Zero-valent iron nanoparticles (INP) were synthesized and stabilized using poly acrylic acid (PAA) to yield stabilized INP (S-INP). A two-dimensional physical model was used to study the fate and transport of the INP and S-INP in porous media under saturated, steady-state flow conditions. Transport data for a nonreactive tracer, INP, and S-INP were collected under similar flow conditions. The results show that unstabilized INP cannot be transported into groundwater systems. On the other hand, the S-INP can be transported like a tracer without significant retardation. However, the S-INP plume migrated downward as it moved horizontally in the physical model, indicating that small density gradients have significant influence on two-dimensional transport. The variable-density groundwater flow model SEAWAT was used to model the observed density-driven transport patterns. This is the first time a two-dimensional transport data set is reported for demonstrating the multidimensional transport characteristics of nanoparticles. The data shows the importance of density effects, which cannot be fully discerned using one-dimensional, column experiments. Finally, we also demonstrate that the numerical model SEAWAT can be used to predict the density-driven transport characteristics of S-INP in groundwater aquifers.

Introduction

Iron nanoparticles are used in a variety of areas for magnetic/electronic, catalytic, and biomedical applications (*1*). In the environmental area, nanoscale iron materials have been widely researched to explore their potential for treating contaminated soil and groundwater (*2*). Among available iron nanoparticles, zero-valent iron nanoparticles (INP) have attracted significant interest due to their ability to reduce a variety of environmental contaminants. For example, INP have been found to degrade chlorinated hydrocarbons such as trichloroethene (TCE), tetrachloroethene (PCE), and carbon tetrachloride (*3, 4*). In addition, environmental contaminants such as perchlorate (*5*), nitrate (*6*), and metals such as Cr(VI) (*7, 8*), lead, nickel, mercury (*2*), arsenic (*9, 10*), and U(VI) (*11*) can be transformed using INP. The INP can also produce hydroxyl radicals in the presence of oxygen to oxidize a variety of organic contaminants such as carbothioate herbicide/molinate (*12*) and benzoic acid (*13*).

* Corresponding Author e-mail: clement@auburn.edu.

Despite its high reactivity, the natural tendency of INP to aggregate, due to its magnetic properties (*14*), may severely limit our ability to be deliver INP into deep porous media formations (*3*). To overcome this limitation, various surface modification and particle stabilization strategies have been developed by using different types of additives such as surfactant (Tween-20) (*15*), poly acrylic acid (PAA) (*16, 17*), carboxymethyl cellulose (CMC) (*18*), cellulose acetate (*19*) starch (*20*), noble metals (*21*), and oil emulsions (*22*). A majority of these studies used batch experiments to demonstrate the additive's potential to stabilize the INP. However, the transport dynamics of stabilized INP can only be tested under dynamic flow conditions. Only a few studies have explored the transport behavior of S-INP in soil columns. Schrick et al. (2004) studied PAA-stabilized INP and its reactivity in a glass burette (*17*); Kanel et. al (2007) studied surfactant (Tween 20) stabilized INP (*15*) and PAA-stabilized INP (*16*) in a sand column and in a glass-bead packed column, respectively. They also studied the reactivity of various forms of stabilized INP for removing arsenic species. All of the above INP transport studies were limited to one–dimensional analysis. To the best of our knowledge, transport of S-INP under two-dimensional flow conditions has not been reported in the literature. Furthermore, there have been no studies on numerical modeling of the observed transport characteristics of INP in groundwater systems.

In this study, we hypothesize that two-dimensional physical models can be used to unravel the multidimensional transport dynamics of S-INP, which may be influenced by small density gradients. We use a novel experimental setup to demonstrate the importance of density effects while injecting nanoparticles into saturated aquifer formations. We compare the two-dimensional transport data of S-INP and INP plumes against a tracer plume to demonstrate the efficiency of the stabilization process. Finally, we use the numerical model SEAWAT to test whether the observed S-INP plume can be conceptually modeled as a density-driven conservative plume.

Materials and Methods

All the chemicals used in the experiments were reagent-grade. Chemicals such as $NaBH_4$ and PAA were obtained from Sigma-Aldrich Chemical Co. (Sigma-Aldrich, St. Louis, MO). Ferrous iron ($FeSO_4.7H_2O$), was obtained from Fisher Chemical Company (Fisher Scientific, Fairlawn, NJ). The porous media selected for this study was A-110 silica beads obtained from Potters Industries (Malverne, PA). The mean bead diameter was 1.1 mm with a variation of $\pm$ 0.1 mm. The porous medium properties were estimated using methods reported in our previous work (*23*). The average porosity of the packed system was estimated to be 0.385. The average hydraulic conductivity was estimated to be 1050 m/day from in situ flow and head measurements. The value of longitudinal dispersivity was estimated to be 1 mm from tracer experiments. Non reactive dye (FD&C Red 40) was used as an optical tracer in all the experiments. Transport characteristics of this dye have been verified in previous experiments where it has been used to visualize the movements of nonreactive solutes (*23*). Ultrapure (18 Ωcm) deionized water purified by a Barnstead purification system was used to prepare all nanoparticles suspensions.

A two-dimensional flow container, shown in Figure 1, was used as the physical model to conduct experiments. The dimensions of the flow container are: 50 cm (length) $\times$ 2 cm (width) $\times$ 28.5 cm (height). Two chambers (5 cm wide) were

10.1021/es071774j CCC: $40.75 © 2008 American Chemical Society
Published on Web 12/21/2007

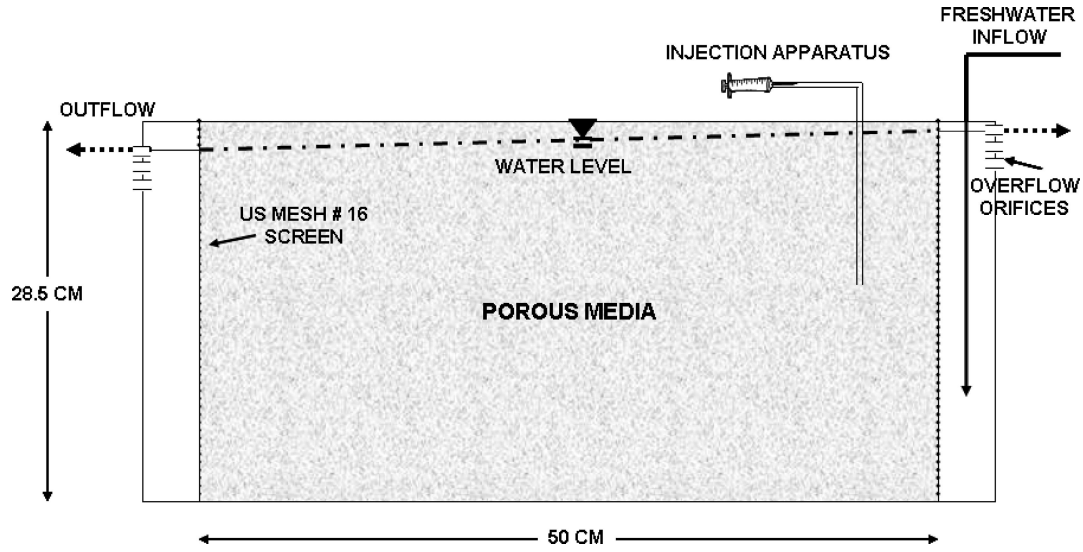

FIGURE 1. Conceptual diagram of the flow container.

TABLE 1. Parameters Used in the Numerical Models

model	parameter	value
General model parameters	grid size (x direction)	0.50 cm
	grid size (z direction)	0.50 cm
	grid size (y direction)	2.00 cm
	number of columns (x)	101
	number of rows (y)	1
	number of layers (z)	44
	number of Stress periods	3
	porosity	0.385
MODFLOW parameters	constant head in the left chamber	22.0 cm
	constant head in the right chamber	22.7 cm
	head convergence criterion	10^{-4}
	advection package	TVD
	concentration convergence criterion	10^{-6}
MT3DMS parameters	transport time step	controlled by a Courant number of 1 and limited to a maximum of 1 s
	longitudinal dispersivity	0.10 cm
	transverse dispersivity	0.01 cm

built at the two ends (left and right) of the container to set constant-head boundary conditions. A series of overflow orifices were drilled in the left and right chambers of the flow container. These overflow orifices allowed excess fluid to drain from the system and also controlled the water level (head) in the chamber. In all the experiments the ambient freshwater flowed from right to left by establishing a head difference of 0.7 cm (gradient of 1.4%) between the head chambers. The flow was allowed to reach steady state for a period of 10 min before starting the injection experiments.

Tracer Test. After establishing stead-state flow conditions, 20 mL of freshwater colored with an optical tracer (red dye) was injected into the porous media to characterize the movement of freshwater in the physical system. The location of the injection point was approximately 15 cm from the right end and 16 cm from the bottom of the inner dimensions of the flow container. It took approximately 16 s to manually inject 20 mL of tracer (at the rate 1.25 mL/s). The transport of the tracer was recorded for about 15 min by taking high resolution digital pictures at regular intervals. Similar data collection techniques were previously employed to study the migration patterns of dense plumes in porous media systems (*24*).

Preparation of INP and S-INP. INP and S-INP were synthesized using previously reported methods with minor modifications (*10, 15, 16*). In this study, 3.25 g of $FeSO_4 \cdot 7H_2O$ and 3.05 g of poly(acrylic acid) (PAA), $(C_3H_4O_2)$ mol wt.: 1800 g/mol, were dissolved in 100 mL of deionized water. The metal salts were reduced by adding 2 g of $NaBH_4$ dissolved in 50 mL deionized water under nitrogen environment. The total concentration of nano-Fe obtained was 4 g/L, which was measured using an atomic absorption spectrophotometer (Spectra AA 220 FS). The density of S-INP suspension was 1.036 g/cm^3 and the pristine INP suspension was 1.030 g/cm^3. The surface area of INP and S-INP preparations synthesized using this approach is expected to be in the range of $\sim$ 15–30 m^2/g (*10, 17*). INP and S-INP were freshly prepared prior to each transport experiment. Similar to the tracer test, 20 mL of 4 g/L INP and S-INP were injected separately into the system using the procedure described earlier. Digital images were taken every minute for a total time of 14 min to record the movement of the nanoparticle plumes.

Modeling Tracer and S-INP Transport Processes. Computer modeling of the data sets obtained from the experiments described above requires the capability to solve both the groundwater flow and transport equations. Our characterization studies indicated that the INP and S-INP solutions are denser than water and hence flow and transport had to be solved simultaneously in a coupled mode. In the groundwater literature, it is a common practice to solve the flow and transport problems independently by assuming that changes in the concentration field have no effect on the flow field (*25*). This assumption may not hold for our experiments since the small-scale density gradients introduced by the dense INP plume may influence the groundwater flow patterns. Accurate numerical simulation of density-dependent flow systems requires the ability to solve variable-density flows. Several types of variable-density modeling codes have been reported in the literature. Among available codes, the most widely used numerical codes are the U.S. Geological Survey public-domain codes SUTRA (*26*) and SEAWAT (*27*). We selected SEAWAT for simulating our experimental results. The variable-density flow and transport code SEAWAT uses a modified form of the MODFLOW code (*25*) to solve the

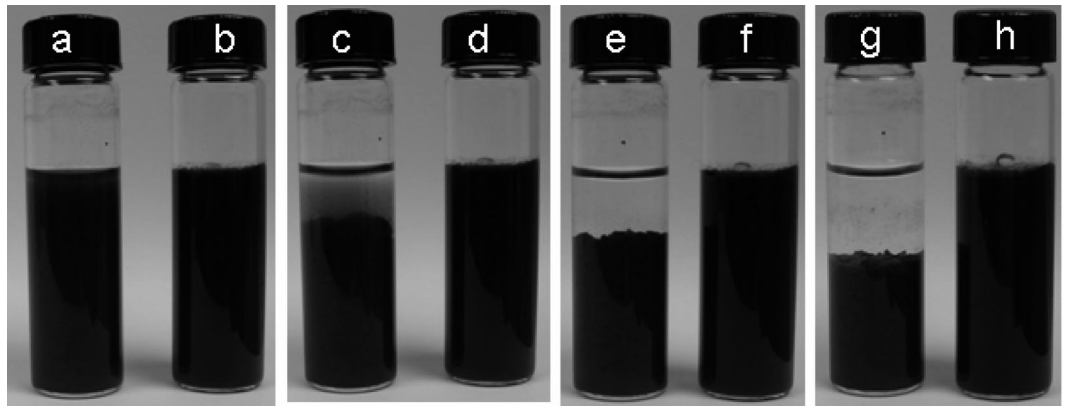

FIGURE 2. Vials containing INP and S-INP at various times: (a) and (b) INP and S-INP after 1 min, (c) and (d) after 10 min, (e) and (f) after 2 h, (g) INP after 2 days, and (h) S-INP after 60 days.

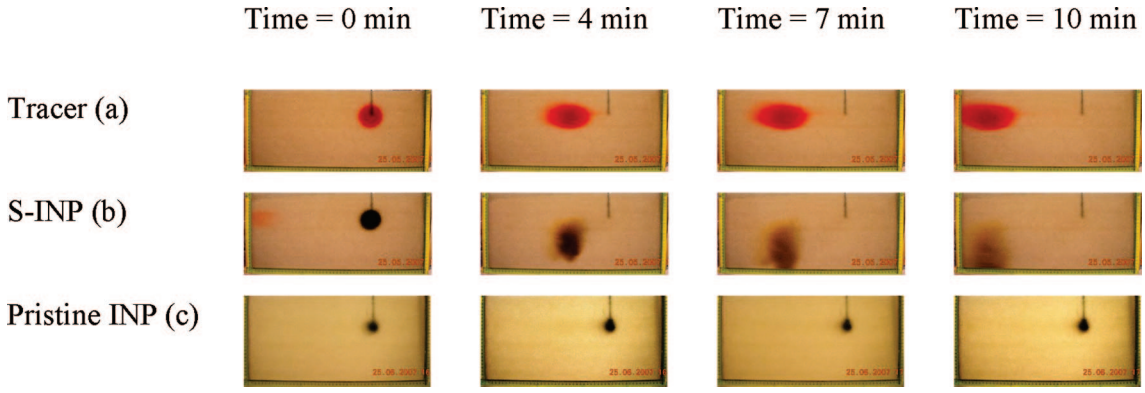

FIGURE 3. Transport of tracer, pristine INP, and S-INP in the flow container.

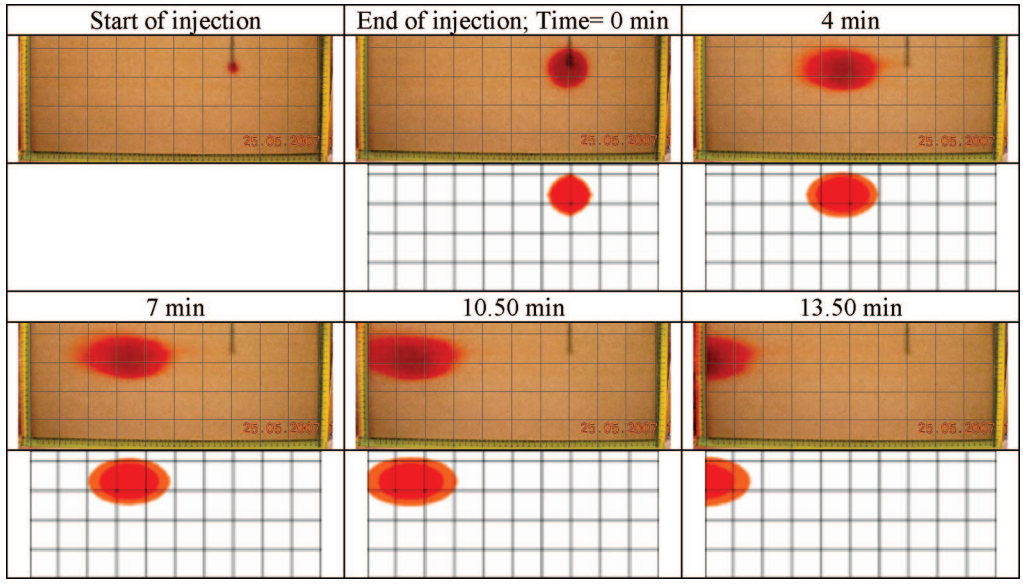

FIGURE 4. Comparison of experimental and numerical modeling results for tracer-dye transport. Numerical results show 1 and 10% shaded contour levels.

groundwater flow equations and the MT3DMS (*25*) code to solve the transport equations and to simulate the associated density-coupling effects.

We chose a constant grid size of 0.5 cm in our numerical model. Constant head boundaries were set up on the right and left end of the numerical model to describe the head gradient used in the experiments. The model discretization and other general transport parameters are summarized in Table 1. Three stress periods were employed to simulate (1) the initial steady-state before injection, (2) injection of tracer or nanoparticles in the domain, and (3) transport of tracer and nanoparticles through the domain. To obtain the steady-state flow conditions, the first stress period was run with constant head boundaries for 200 s. The second stress period was run for 16 s; during this period, 20 mL of tracer or nanoparticles solution was injected into the system through a well assuming a constant flow rate of 1.25 mL/s. The well was turned off in the third stress period to simulate the transport of tracer or nanoparticles. Since the transport was highly advection dominated in our experiments, we used the total variation diminishing (TVD) technique to solve the

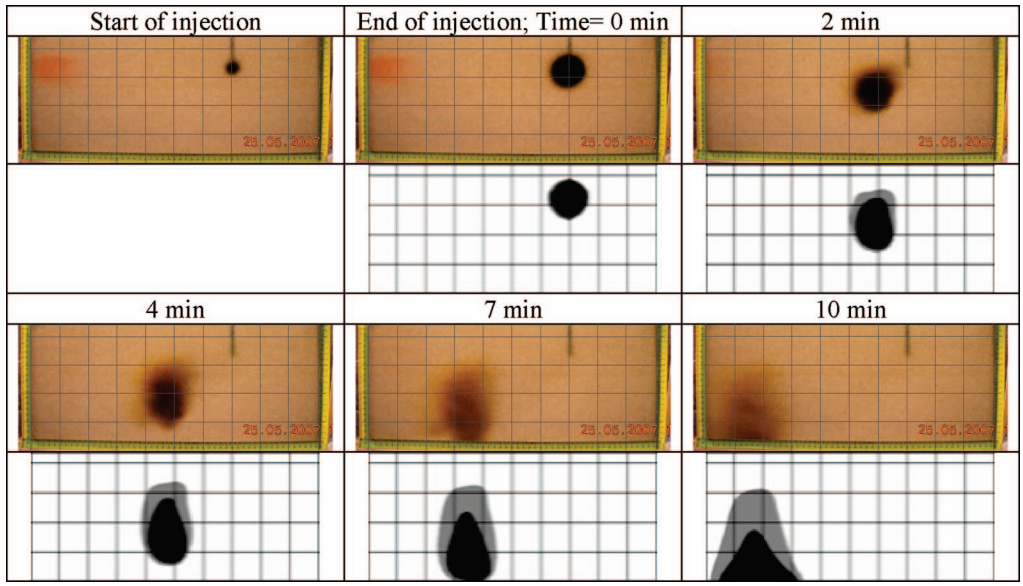

FIGURE 5. Comparison of experimental and numerical modeling results for S-INP transport. Numerical results show 1 and 10% shaded contour levels.

advection part of the transport equation. This technique helps to minimize numerical dispersion effects (*25*).

Results and Discussion

Stability of INP and S-INP in vVials. Figure 2 shows the digital pictures of the vials containing pristine INP and S-INP dispersed in the aqueous phase. The pictures show that INP started to aggregate and settled in the vials within 1–10 min (Figure 2a and c). The INP suspension was well segregated and the particles settled at the bottom of vial after 2 days (Figure 2g). However, S-INP was well dispersed and remained as a homogeneous gray-colored solution for up to 60 days (Figure 2h). This qualitative data demonstrates that the stabilizer (PAA) kept the particles suspended.

Transport of INP and S-INP in Porous Media. The transport patterns of the tracer, pristine INP and S-INP observed at different time intervals are shown in Figure 3. The pictures in the first column (time = 0 min) of Figure 3 present the location of the plumes just after injection into the porous medium. The other pictures in the figure were taken at the following times: 4, 7, and 10 min. The data indicates that the colored freshwater tracer dispersed and moved horizontally and reached the left boundary in approximately 10 min (see Figure 3a). However, S-INP moved vertically downward toward the bottom of the flow container as it migrated horizontally toward the left boundary (see Figure 4b). The downward movement of S-INP particles is due to the higher density of S-INP (1.036 g/cm^3) compared with water (1 g/cm^3). Pristine INP, on the other hand, showed no transport even after 10 min, as indicated by Figure 4c. The pristine INP is expected to have positive charge at neutral pH; whereas, the porous medium will be negatively charged. Therefore, INP can attach to the porous medium and become immobilized because of charge interactions. Furthermore, there are other physical processes that can immobilize both INP and S-INP in porous media systems. It is reported in the literature that INP transport can be affected by three distinct transport mechanisms including diffusion, interception, and sedimentation (*17, 28*). Lecoanet et al. (2004) reported that the transport of different nanomaterials (fullerene, single wall nanotube, alumoxane, C_{60}, and ferroxane) in a glass bead column was influenced by both hydrophobic and hydrophilic interactions, blocking of deposition sites, and changes in the attachment efficiency due to ionic strength and steric stabilizations (*29, 30*).

Interestingly, our S-INP transport data did not show much retardation when compared to the tracer data. The higher mobility of S-INP particles can be explained by the association of the hydrophobic part of the PAA with INP and the orientation of the polar headgroup toward the aqueous phase (*15*). Furthermore, unlike INP (which will be positively charged), the S-INP suspension will be negatively charged at neutral pH since it was stabilized using an anionic polymer (*16, 17*). Hence, one can expect very little interaction between S-INP and the porous medium (glass beads). In this study, we hypothesized that the observed S-INP transport was primarily controlled by advection and dispersion processes that are coupled to small-scale density gradients. In the section below we provide numerical calculations to test the validity of this hypothesis.

The experimental observations were simulated using the variable-density flow code SEAWAT. The results obtained from the numerical model (1 and 10% shaded contour levels) are compared with the experimental results in Figures 4 and 5. Figure 4 compares SEAWAT results against the tracer data and the results show that the model was able to capture the transport patterns very well. Figure 5 compares SEAWAT results against S-INP transport data. The model simulations employed a retardation factor value of unity. Therefore, other than the standard advection dispersion processes, the density coupled transport effects is the only additional process included in the simulation. The figure shows that the numerical model was able to accurately predict the sinking effects of the plume and also the overall shape of the plume. These results indicate that our assumption of modeling S-INP transport as a conservative dense plume was indeed correct, and small-scale density gradients can play a significant role in transporting S-INP.

In this study we have provided two-dimensional transport data which show that the standard INP is virtually immobile, whereas the PAA-stabilized INP can be transported without any significant retardation. To the best of our knowledge, there is no data set available in the published literature that demonstrates the transport behavior of stabilized nanoparticles in a two-dimensional setting. The two-dimensional data set also indicates that density-driven flow can play an important role in transporting certain classes of nanoparticles into deeper aquifer regions. Since these density-driven sinking effects cannot be fully discerned from conventional one-dimensional column experiments, it is important to

characterize nanoparticle transport in multidimensional systems. Our modeling results show that the density-coupled groundwater flow model SEAWAT can be used to predict the movement of S-INP, and hence, the model can potentially be used as a tool for designing nanoparticle injection experiments. However, it is important to note that the physical and chemical heterogeneities inherently present in field soils can interact with S-INP resulting in filtration and clogging of the particles. Therefore, carefully designed feasibility studies should be completed using site soils prior to any field-scale INP injection experiments.

Acknowledgments

This research was supported by the office of science (BER), U.S. Department of Energy Grant No. DE-FG02-06ER64213. We would like to thank the reviewers and editors for their detailed comments and suggestions.

Literature Cited

(1) Huber, D. L. Synthesis, properties and applications of iron nanoparticles. *Small* **2005**, *1*, 482–501.
(2) Li, L.; Fan, M.; Brown, R. C.; Leeuwen, J. H. V.; Wang, J.; Wang, W.; Song, Y.; Zhang, P. Synthesis, properties and environmental applications of nanoscale iron-based materials: A review. *Crit. Rev. Environ. Sci. Technol.* **2006**, *36*, 405–431.
(3) Nurmi, J. T.; Tratnyek, P. G.; Sarathy, V.; Baer, D. R.; Amonette, J. E.; Pecher, K.; Wang, C.; Linehan, J. C.; Matson, D. W.; Penn, R. L.; Driessen, M. D. Characterization and properties of metallic iron nanoparticles: Spectroscopy, electrochemistry, and kinetics. *Environ. Sci. Technol.* **2005**, *39*, 1221–1230.
(4) Zhang, W.-X. Nanoscale Iron Particles for Environmental Remediation: An Overview. *J. Nanopart. Res.* **2003**, *5*, 323–332.
(5) Cao, J.; Elliott, D.; Zhang, W.-X. Perchlorate Reduction by Nanoscale Iron Particles. *J. Nanopart. Res.* **2005**, *7*, 499–506.
(6) Gordon, C. C.; Yang, G. C.; Lee, H.-L. Chemical reduction of nitrate by nanosized iron: kinetics and pathways. *Water Res.* **2005**, *39* (5), 884–894.
(7) Ponder, S. M; Darab, J. G.; Mallouk, T. E. Remediation of Cr(VI) and Pb(II) aqueous solutions using supported, nanoscale zero-valent iron. *Environ. Sci. Technol.* **2000**, *34*, 2564–2569.
(8) Manning, B. A.; Kiser, J. R.; Kanel, S. R. Spectoscopic investigation of Cr(III)- and Cr(VI)-treated nanoscale zerovalent iron. *Environ. Sci. Technol.* **2007**, *41*, 586–592.
(9) Kanel, S. R.; Grenèche, J. M.; Choi, H. Arsenic (V) removal from groundwater using nano scale zero-valent iron as a colloidal reactive barrier material. *Environ. Sci. Technol.* **2006**, *40*, 2045–2050.
(10) Kanel, S. R.; Manning, B.; Charlet, L.; Choi, H. Removal of arsenic(III) from groundwater by nanoscale zero-valent iron. *Environ. Sci. Technol.* **2005**, *39*, 1291–1298.
(11) Burghardt, D.; Kassahun, A. Development of a reactive zone technology for simultaneous in situ immobilisation of radium and uranium. *Environ. Geol.* **2005**, *49*, 314–320.
(12) Joo, S. H.; Feitz, A. J.; Waite, T. D. Oxidative degradation of the carbothioate herbicide, molinate, using nanoscale zero-valent iron. *Environ. Sci. Technol.* **2004**, *38*, 2242–2247.
(13) Joo, S. H.; Feitz, A. J.; Sedlak, D. L.; Waite, T. D. Quantification of the oxidizing capacity of nanoparticulate zero-valent iron. *Environ. Sci. Technol.* **2005**, *39*, 1263–1268.
(14) Phenrat, T.; Saleh, N.; Sirk, K.; Tilton, R. D.; Lowry, G. V. Aggregation and sedimentation of aqueous nanoscale zerovalent iron dispersions. *Environ. Sci. Technol.* **2007**, *41*, 284–290.
(15) Kanel, S. R.; Nepal, D.; Manning, B.; Choi, H. Transport of surface-modified iron nanoparticle in porous media and application to arsenic(III) remediation. *J. Nanopart. Res.* **2007**, *9*, 725–735.
(16) Kanel, S. R.; Choi, H. Transport characteristics of surface-modified nanoscale zero-valent iron in porous media. *Water Sci. Technol.* **2007**, *55*, 157–162.
(17) Schrick, B.; Hydutsky, B. W.; Blough, J. L.; Mallouk, T. E. Delivery vehicles for zerovalent metal nanoparticles in soil and groundwater. *Chem. Mater* **2004**, *16*, 2187–2193.
(18) He, F.; Zhao, D.; Liu, J.; Roberts, C. B. Stabilization of Fe−Pd nanoparticles with sodium carboxymethyl cellulose for enhanced transport and dechlorination of trichloroethylene in soil and groundwater. *Ind. Eng. Chem. Res.* **2007**, *46*, 29–34.
(19) Wu, L.; Shamsuzzoha, M.; Ritchie, S. M. C. Preparation of cellulose acetate supported zero-valent iron nanoparticles for the dechlorination of trichloroethylene in water. *J. Nanopart. Res.* **2005**, *7*, 469–476.
(20) He, F.; Zhao, D. Preparation and characterization of a new class of starch-stabilized bimetallic nanoparticles for degradation of chlorinated hydrocarbons in water. *Environ. Sci. Technol.* **2005**, *39*, 3314–3320.
(21) Elliott, D. W.; Zhang, W. X. Field assessment of nanoscale bimetallic particles for groundwater treatment. *Environ. Sci. Technol.* **2001**, *35*, 4922–4926.
(22) Quinn, J.; Geiger, C.; Clausen, C.; Brooks, K.; Coon, C.; O'Hara, S.; Krug, T.; Major, D.; Yoon, W.-S.; Gavaskar, A.; Holdsworth, T. Field demonstration of DNAPL dehalogenation using emulsified zero-valent iron. *Environ. Sci. Technol.* **2005**, *39*, 1309–1308.
(23) Goswami, R. R.; Clement, T. P. Laboratory-scale investigation of saltwater intrusion dynamics. *Water Resour. Res.* **2007**, *43*, W04418, DOI: 10.1029/2006WR005151.
(24) Oostrom, M.; Hayworth, J. S.; Dane, J. H.; Guven, O. Behaviour of dense aqueous phase leachate plumes in homogenous porous media. *Water Resour. Res.* **1992**, *28* (8), 2123–2134.
(25) Zheng, C.; Bennett, G. *Applied Contaminant Transport Modeling*; Wiley Interscience: Hoboken, NJ, 2002.
(26) Voss, C. I.; Souza, W. R. Variable density flow and solute transport simulation of regional aquifers containing a narrow fresh-water-saltwater transition zone. *Water Resour. Res.* **1987**, *23*, 1851–1866.
(27) Langevin, C. D.; Guo, W. X. MODFLOW/MT3DMS-based simulation of variable-density ground water flow and transport. *Ground Water* **2006**, *44*, 339–351.
(28) Tufenkji, N.; Elimelech, M. Correlation equation for predicting single-collector efficiency in physicochemical filtration in saturated porous media. *Environ. Sci. Technol.* **2004**, *38*, 529–536.
(29) Lecoanet, H. F.; Bottero, J. Y.; Wiesner, M. R. Laboratory assessment of the mobility of nanomaterials in porous media. *Environ. Sci. Technol.* **2004**, *38*, 5164–5169.
(30) Lecoanet, H. F.; Wiesner, M. R. Velocity effects on fullerene and oxide nanoparticle deposition in porous media. *Environ. Sci. Technol.* **2004**, *38*, 4377–4382.

ES071774J